

# Journal of Materials Chemistry A

Accepted Manuscript



This is an *Accepted Manuscript*, which has been through the Royal Society of Chemistry peer review process and has been accepted for publication.

*Accepted Manuscripts* are published online shortly after acceptance, before technical editing, formatting and proof reading. Using this free service, authors can make their results available to the community, in citable form, before we publish the edited article. We will replace this *Accepted Manuscript* with the edited and formatted *Advance Article* as soon as it is available.

You can find more information about *Accepted Manuscripts* in the [Information for Authors](#).

Please note that technical editing may introduce minor changes to the text and/or graphics, which may alter content. The journal's standard [Terms & Conditions](#) and the [Ethical guidelines](#) still apply. In no event shall the Royal Society of Chemistry be held responsible for any errors or omissions in this *Accepted Manuscript* or any consequences arising from the use of any information it contains.

## PAPER

## Long-lasting antibacterial behavior of a novel mixed matrix water purification membrane

Qianqian Zhao <sup>a</sup>, Jingwei Hou <sup>b</sup>, Jiangnan Shen <sup>c</sup>, Jindun Liu <sup>a</sup>, Yatao Zhang <sup>a, b\*</sup>

Received  
Accepted

www.rsc.org/

Membrane fouling by microbial and organic components is considered as the “Achilles heel” of membrane process as it not only reduces the membrane performance but also leads to membrane biodegradation. In this work, a novel high flux, antibacterial and antifouling ultrafiltration membrane was fabricated by blending silver nanoparticles (AgNPs)-halloysite nanotubes (HNTs)-reduced graphene oxide (rGO) nanocomposite (AgNPs-HNTs-rGO) into polyethersulfone (PES) membrane matrix. HNTs were applied to expand the interlayer space between neighboring rGO sheets and eliminate the leaching on AgNPs. The hybrid membranes had higher hydrophilicity, surface smoothness and higher water permeation flux when compared with pure PES membrane. Both dynamic and static BSA adsorption tests revealed improved antifouling behavior of the hybrid membrane. In addition, the incorporated AgNPs were evenly attached onto the rGO support with an average size of 10 nm, which ensured its good antibacterial performance: the hybrid membrane had an ideal bacteriostasis rate against *Escherichia coli* (*E. coli*) even after six months storage.

### Introduction

The membrane based water filtration processes have been widely applied in water and wastewater treatment.<sup>1-4</sup> However, the biofouling of the membranes, initiated with the bacterial growth on membrane surface and followed by the release of extracellular polymeric substances (EPS, mainly polysaccharide) and the formation of a thick biofilm, increases the operational cost and deteriorates the stable performance of the membrane filtration system.<sup>5</sup> The formation of the bacteria biofilm would reduce the water flux. Currently, the membrane biofouling mitigation approaches include chemical cleaning and pretreatment. However, the operational cost and the lifespan of the membrane will be negatively affected. Therefore, the research to develop antibacterial membranes has attracted increasing attention. The formation of biofilm is initiated with the cell adhesion and growth on the membrane surface. Therefore, it is important to prevent the cell adhesion or to inhibit its growing activity onto the membrane surface. The incorporation of antibacterial nanomaterials, such as Ag<sup>6,7</sup> or Ag<sup>+</sup><sup>8</sup>, Cu<sup>2+</sup><sup>9</sup>, TiO<sub>2</sub><sup>10</sup>, chitosan<sup>11</sup> and polycations<sup>12,13</sup>, into membranes provides an potential solution to develop the anti-biofouling membrane. Among different nanofillers, the application of silver nanoparticles has received considerable attention due to their excellent antibacterial activities, low toxicity to human and broad antibacterial spectrum to different kinds of bacteria cells.<sup>14</sup> Previously, it was believed the main antibacterial mechanism of Ag was based on Ag ions. In aqueous environment, the Ag metal could release ionic Ag, which further reacts with thiol groups to form S-Ag or disulfide bonds, damaging the peptides of the bacterial proteins and dimerizing the DNA of bacteria.<sup>15</sup> Recently, it was also

discovered the Ag nanoparticle itself can damage the cell wall, increase in bacterial cellular membrane permeability, and eventually lead to the death of the cell and the release of the intracellular material.<sup>16</sup> In contacting with Ag nanoparticles, bacterial cells will take in Ag ions, which immediately inhibits enzymes involved in the respiration pathways, generates the reactive oxygen species and eventually damages the cell.<sup>17</sup> Therefore, the incorporation of Ag nanoparticles in polymer membrane matrix could suppress the bacteria growth on the membrane surface and potentially mitigate the membrane biofouling. However, it is demonstrated that the antibacterial properties of the Ag nanoparticles are strongly associated with its size and shape: the particles with 1-10 nm have the most significant antibacterial properties.<sup>18</sup> However, the aggregation of Ag nanoparticles, a common phenomenon in the mixed matrix membrane, negatively affects the antibacterial activities. Another problem associated with the mixed matrix membrane was the gradual loss of the incorporated nanomaterials during the membrane filtration process.<sup>19</sup> As a result, the long-term effectiveness of the anti-biofouling membrane will be compromised.<sup>20</sup> Therefore, it is crucial to achieve stable incorporation of nanosilver inside the membrane matrix with minor aggregation.

On the other hand, even through the nanosilver mixed matrix membrane has good anti-biofouling effect, and they may still suffer from membrane fouling induced by natural organic matter (NOM). During the membrane water filtration process, the NOM adsorption or desorption may occur, forming cake layer on membrane surface and plugging inside membrane pores. For the Ag incorporated anti-biofouling membranes, the rupture of the bacterial cell and the leakage of intracellular components occur near membrane surface, and the released intracellular substance may have higher tendency to form

## ARTICLE

membrane fouling.<sup>21</sup> Currently, the most acknowledged approaches to mitigate membrane fouling by organic matter are to increase membrane hydrophilicity and smoothness.<sup>22</sup> However, simply adding Ag nanoparticle could not address these issues. Currently, membrane surface modification has been intensively investigated to promote the membrane antifouling performances,<sup>23</sup> including surface coating,<sup>24-26</sup> graft polymerization<sup>27,28</sup> and interfacial polymerization<sup>29,30</sup>. Blending nanoscale hydrophilic additives is another straightforward and effective approach to improve the antifouling behavior of the membrane. So far different nanofillers have been tested which include but not limited to TiO<sub>2</sub><sup>31,32</sup>, SiO<sub>2</sub><sup>33-36</sup>, boehmite<sup>37</sup>, Al<sub>2</sub>O<sub>3</sub><sup>38</sup>, and carbon nanotubes<sup>32,39,40</sup>. Compared with the surface modification techniques, the blending process is easy to operate and most feasible for large scale industrial production.<sup>41</sup> Therefore, it is critical to develop advanced membranes which can suppress the growth of bacteria, have good antifouling properties and tailored separation ability to satisfy various applications.<sup>42</sup> The application of graphene oxide (GO), a two-dimensional carbon material with plentiful oxygen-containing groups, together with membrane technology has attracted great attention lately due to its large surface area and hydrophilicity. Recently, the antibacterial properties of GO and reduced GO (rGO) have been discovered,<sup>43-45</sup> and the GO based nanocomposite antibacterial membranes have been studied.<sup>46</sup> The carbon-based nanomaterials induces bacterial cytotoxicity towards *Escherichia coli* (*E. Coli*), *Pseudomonas aeruginosa*, *Bacillus subtilis* and *Staphylococcus epidermis*.<sup>17</sup> Furthermore, several studies have been carried out on the synergistic antibacterial effect of GO and Ag nanoparticles. The formation of the GO-Ag nanocomposite possesses enhanced antibacterial properties and antifungal activities. The large surface area of GO sheets allows high Ag nanoparticle loading, and the layer structure of the GO also stabilizes the Ag nanoparticles against unwanted aggregations, both beneficial towards the antibacterial property of the Ag nanoparticles.<sup>47,48</sup> In our previous work, GO nanosheets were incorporated into polyethersulfone (PES) ultrafiltration membranes via blending process. Although improved antibacterial and antifouling properties were observed, the addition of GO resulted in higher intrinsic membrane resistance due to the tight GO sheets structure inside the membrane matrix. A potential solution is to strategically locate nanoscale spacers between the neighboring GO sheets to form nanoscale flow channels for water. Recently, we have developed a series of halloysite nanotubes (HNTs), a type of hydrophilic inorganic nanotubes, based mixed matrix membranes with improved antifouling and antibacterial performance.<sup>49-51</sup> The presence of HNTs in the membrane matrix could minimize the leaching of Ag nanoparticles during water filtration which could benefit the long-term antibacterial performance.<sup>7,52</sup> Recently, we synthesized a novel sandwich-like nanocomposite antibacterial reagent by growing Ag nanoparticles on the surface of graphene-HNTs nanostructures. The resulted reagent possessed improved antibacterial capability against *E. coli* and *S. aureus* over the individual Ag nanoparticles, graphene or Ag/graphene nanocomposites. In addition, the formed sandwiched structure can potentially provide extra nanoscale flow channels for water. With this respect, the incorporation of such sandwich-like nanocomposite into membrane could potentially promote the water permeation flux. However, little research has been devoted to integrate the graphene, HNTs and AgNPs together for advanced membrane fabrication, and the dispersion of the graphene based nanocomposite inside a membrane would be challenging due to the hydrophobic nature of the material.

In this study, a sandwich-like nanocomposite material was synthesis with Ag nanoparticles (AgNPs), halloysite nanotubes (HNTs) and

reduced GO nanosheets (rGO). Then a series of hybrid membrane was fabricated by blending different amount of the above nanocomposite into the polyethersulfone membrane matrix. Comprehensive characterization techniques were applied to understand the effect of the nanocomposite on membrane morphology, hydrophilicity, water filtration performance and pore size of the hybrid membrane. In addition, the antifouling performance of the hybrid membrane was examined with both dynamic and static protein adsorption test. Furthermore, a series tests were carried out to understand the antibacterial behavior of the hybrid membrane, especially after long-term storage and repeated use.

## Experimental

### Materials

Graphite powders (spectral pure) were purchased from Sinopharm Chemical Reagent Co., Ltd., and were used as received. Hyperbranched polyethylenimine (HPEI) (average MW 25000), 1-Ethyl-3-(3-dimethylamino-propyl) carbodiimide hydrochloride (EDC-HCl) and N-hydroxy-succinimide (NHS) were purchased from Sigma Aldrich and used without further purification. Polyethersulfone (PES, Ultrason E6020P with MW 58 kDa) was obtained from BASF, Germany. Halloysite clay from Henan Province (China) was milled and sieved to obtain HNTs. 1, 6-hexamethylene diisocyanate (HMDI) was obtained from Acros. Dibutyltin dilaurate was supplied by TCI Shanghai. All the other chemicals (analytical grade) were obtained from Tianjin Kermel Chemical Reagent Co., Ltd. China, and were used without further purification. Deionized water was used in this study for all the experiments.

### Synthesis of Ag, HNTs and rGO based nanocomposite materials

The synthesis process includes the modification of GO, HNTs and the final preparation of the nanocomposite material.

GO was prepared by oxidizing natural graphite.<sup>53</sup> The as-prepared GO (200 mg) was distributed in phosphate buffer solution (200 mL, pH=6.86) to obtain a homogeneous dispersion with the aid of ultrasonication in a water bath (KH-100,100 w). Then HPEI (1.0 g), EDC-HCl (400 mg) and NHS (240 mg) were added under constant stirring.<sup>54</sup> After reaction for 24 h at room temperature, the precipitate was collected by centrifugation (8000 rpm) for 5 min and re-suspension for three times to remove un-reacted chemicals. Finally, the black powder was collected and vacuum-dried under room temperature.

Prior to modification, HNTs was fully dried at 300°C for 5 h. Chemical modification of HNTs by succinic anhydride was carried out applying the following procedures: dried HNTs powder (2 g) was poured into acetone (60 g), and the suspension was thoroughly dispersed after 30 min ultrasonication. Then, dibutyltin dilaurate (0.5 mL), used as catalyst, was dissolved in the solution by shaking and the suspension was stirred for 30 min in N<sub>2</sub> atmosphere to make sure the reaction in water free condition. Thereafter, HMDI (5 g) was added into the suspension which was refluxed at 70°C for 4 h under constant stirring. The products were collected by centrifugation (6000 rpm) for 5 min and washed with acetone for several times and were dried in a vacuum drying chamber at 60 °C.

The interim HNTs bound HMDI (HNTs-HMDI) was first modified with succinic anhydride. Dried HNTs-HMDI powder (1.5 g) was added in 60 g acetone and dispersed under ultrasonication for 30 min. Next, dibutyltin dilaurate (0.5 mL) was added into the solution and then the suspension was stirred for 30 min in N<sub>2</sub> atmosphere to conduct the reaction under water free condition. Subsequently,

succinic anhydride (2.24 g) was added and the suspension was refluxed at 70°C for 4 h under constant stirring. The final products were collected by centrifugation (6000 rpm) for 5 min and washed with acetone for several times, then dried in a vacuum oven at 60°C. The modified HNTs (10 mg) was distributed in 250 mL phosphate buffer solution (pH=6.86) to obtain a homogeneous dispersion under ultrasonication. Then, 400 mg of EDC-HCl and 240 mg of NHS were added under constant stirring. After reaction for 5 min, 100 mg of modified GO was added and dispersed uniformly under ultrasonication. Finally, the mixture solution was left for 24 h at room temperature. Up to the completion of above reaction, the Ag nanoparticles were immobilized. 50 mg of AgNO<sub>3</sub> was added to the above-mentioned mixture system with high speed stirring. After reaction for 2 h, 3 mg of NaBH<sub>4</sub> was added dropwisely and reacted for another 4 h at room temperature to reduce silver ion and GO nanosheets. The resulted mixture was centrifuged (5000 rpm) for 5 min and then re-suspended with ethanol for several times and eventually vacuum-dried at 60°C. The reaction principle of AgNPs-HNTs-rGO nanocomposites is shown in Fig. 1. The resulted nanocomposite material was marked as AgNPs-HNTs-rGO in this work.

### Membrane preparation

All the membranes were prepared *via* classical phase inversion method. The casting solutions contained 18 wt.% PES, 8 wt.% PVP, 0.8 wt.% acetone, and dimethylacetamide (DMAc) as the solvent. Different amounts of AgNPs-HNTs-rGO (based on the content of PES) were added to evaluate the effect of the nanocomposite material loading on the membrane performance. In this work, up to 3 wt.% of the nanocomposite was added as further increase its concentration would lead to high membrane casting solution viscosity and make the membrane casting difficult. After degassing the casting solution overnight, the membrane was prepared with a hand-casting knife (100 μm of thickness) and then coagulated in deionized water for 24 h. The membrane was further rinsed with deionized water to remove the loosely attached AgNPs-HNTs-rGO and water soluble components in the membrane.

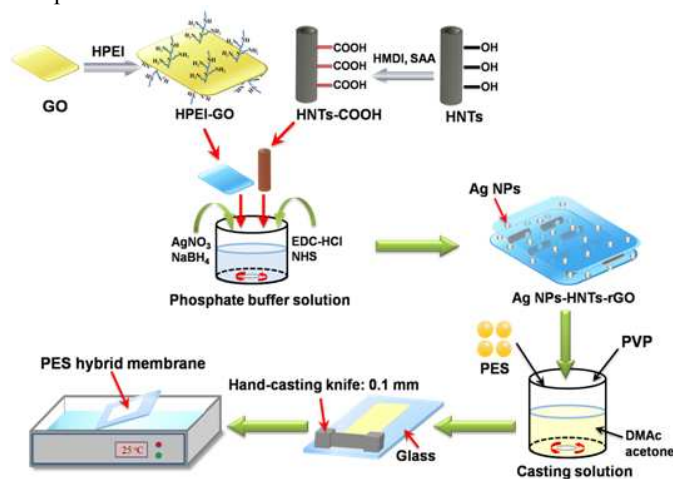


Fig. 1 Reaction principle of preparing AgNPs-HNTs-rGO nanocomposites and PES hybrid membranes

### Characterization of AgNPs-HNTs-rGO

A FEI model TECNAI G<sup>2</sup> transmission electron microscope (200 KV acceleration voltages) was used to examine the structure of AgNPs-HNTs-rGO. Prior to imaging, the samples were well dispersed into solvent under ultrasonication. The suspended particles

were then transferred to a copper grid (400 meshes) coated with a strong carbon film and dried. Energy Dispersive System (EDS) was also carried out in a JEOL JSM-7500F FE-SEM with samples sputtered with gold.

### Characterization of PES membranes

**X-ray photoelectron spectroscopy (XPS).** In order to accurately analyze the content of elements on the membrane surface, X-ray photoelectron spectroscopy (XPS) analysis was performed using a Kratos AXIS Ultra DLD X-ray photoelectron spectrometer with a monochromatized Al K $\alpha$  (15 kV, 10 mA) X-ray source and hemispherical sector analyzer (HSA). For calibration the C 1s peak was used (282.3 eV).

**Dynamic water contact angle.** Dynamic water contact angle ( $\theta$ ) was measured at 25°C and 50% relative humidity on a contact angle system (OCA20, Dataphysics Instruments, Germany). The membrane sample was firstly fixed onto a flat glass plate with double side tape. Deionized water (5 μL) was carefully dropped on the top surface and the contact angle between the water and membrane was measured until no further change was observed. To minimize the experimental error, the contact angle was measured at five random locations for each sample and then the average value was reported.

**Scanning electron microscopy (SEM) and Energy Dispersive System (EDS).** The morphology of the cross section and surface of the membranes were inspected by SEM using a JEOL Model JSM-6700F scanning electron microscope (Tokyo, Japan). Energy Dispersive System (EDS) test was carried out in a JEOL JSM-7500F FE-SEM. All samples were sputtered with gold prior to the test, and the cross-section samples were obtained after fracturing the membrane sample after soaking in liquid nitrogen.

**Separation performance.** A cross flow system was used to characterize the permeation performance of the membrane. A piece of flat sheet membrane with an effective area of 22.2 cm<sup>2</sup> was mounted in the cell. Each membrane was firstly pre-compacted using pure water at 0.2 MPa until a steady flux was obtained (usually after 30 min), and then the pure water flux was recorded at 0.1 MPa under 25°C.

The membrane filtration of PEG was carried out to understand the change of pore size for the nanocomposite membrane. After the pre-compaction, PEG 20000 solution (0.5 g/L) was forced to permeate through the membranes under 0.1 MPa and the permeate solutions were collected. The concentrations of PEG 20000 in the permeate solutions were examined by UV spectrophotometer. The permeation flux ( $J$ ) and rejection ( $R$ ) were calculated using the following equation:

$$J = \frac{V}{A\Delta t} \quad (1)$$

$$R = \left(1 - \frac{C_p}{C_f}\right) \times 100\% \quad (2)$$

Where  $V$  is the volume of permeate pure water (L),  $A$  is the effective area of the membrane (m<sup>2</sup>), and  $\Delta t$  is the permeation time (h),  $C_p$  is the permeate concentration and  $C_f$  is the feed concentration.

**Transmission electron microscopy (TEM).** In order to examine the distribution of the AgNPs-HNTs-rGO in the membranes, transmission electron microscopy (TEM) measurement was carried out with a FEI model TECNAI G<sup>2</sup> transmission electron microscope operated at 200 kV. The membranes were embedded in epoxy resin and cross sections with a thickness of 50 nm were obtained by sectioning with a Leica Ultracut UCT ultramicrotome. Then these thin sections were mounted on the carbon-coated TEM copper grids for examination.

## ARTICLE

**Atomic force microscope (AFM).** For analyzing the surface morphology and roughness of the membranes, atomic force microscopy was employed using the AFM apparatus (DI Nanoscope IIIa, Veeco, USA). Small squares of the prepared membranes (ca. 1 cm<sup>2</sup>) were cut and glued on glass substrate. The membrane surfaces were examined in a scan size of 20 μm×20 μm.

**Porosity.** The porosity of membrane was measured by gravimetric method and calculated according to equation (3):<sup>37</sup>

$$\varepsilon = \frac{m_1 - m_2}{\rho_w A l} \quad (3)$$

Where  $m_1$  is the weight of the wet membrane;  $m_2$  is the weight of the dry membrane;  $\rho_w$  is the water density (0.998 g/cm<sup>3</sup>);  $A$  is the effective area of the membrane (m<sup>2</sup>),  $l$  is the membrane thickness (m).

**Membrane antifouling performance.** In this work, dynamic and static protein adsorption tests were carried out to understand the antifouling performance of the membrane.

For the dynamic adsorption test, after the membrane pre-compaction with pure water, the pure water permeability  $J_0$  was measured. Then 1 g/L BSA solution was applied in the feed side and the permeation flux ( $J$ ) was monitored. Each cycle of BSA permeation test lasted 90 min and final permeation flux was recorded as  $J_p$ . Then the fouled membranes were washed with 0.1 M NaOH solution for 30 min followed by rinsing with deionized water till the pH of water returned neutral. Then the water flux of the cleaned membranes  $J_R$  was measured. Such dynamic BSA adsorption test was carried out for 3 cycles on each membrane. In order to evaluate the antifouling property of membranes, the flux recovery ratio (FRR) and the flux decline rate ( $R_t$ ) were calculated as follows:<sup>37</sup>

$$FRR = \left( \frac{J_R}{J_0} \right) \times 100\% \quad (4)$$

$$R_t = \left( 1 - \frac{J_p}{J_0} \right) \times 100\% \quad (5)$$

Here,  $R_t$  is the degree of total flux loss caused by total fouling. The static protein adsorption of BSA was also conducted to understand the fouling behavior of the membrane. Each membrane (3×3 cm) was soaked in 50 mL BSA phosphate buffer (pH=7, 0.8 g/L) for 24 h at 40°C in a shaker to reach the adsorption equilibrium. The remaining BSA solution in the supernatant was monitored by a UV spectrophotometer device. The adsorption amount was calculated in accordance with equations (6):

$$Q = \frac{(C_0 - C_e) \times V}{A} \quad (6)$$

Where  $Q$  is the adsorption amount of protein (μg/cm<sup>2</sup>),  $C_0$  is the initial concentration of the protein solution (μg/mL),  $C_e$  is the equilibrium concentration of protein (μg/mL),  $V$  is the volume of the added protein solution (mL), and  $A$  is the area of the added membranes (cm<sup>2</sup>).

**Antibacterial activity tests.** The antibacterial activities of the membranes against *E. coli* were tested by SEM and TEM to study the morphology of cells after being treated with the membranes.<sup>48</sup> 100 μL suspension of 10<sup>6</sup> CFU (colony-forming units)/mL *E. coli* cells was placed on an LB agar growth plate. After 1 h at 37 °C, a piece of square membrane was gently placed on the top of the inoculated agar plates to interact cells with materials. Then the growth plates were incubated at 37°C for 12 h. The bacteria cells on membranes were immobilized with 2.5% glutaraldehyde and 1% osmium tetroxide, then the samples were sputter-coated with gold

and imaged under SEM to study the morphology of cells on membranes.

Besides, antibacterial rate was also evaluated with the viable cell count method. The detailed process was as follows: the bacteria was inoculated in 5 mL of LB liquid nutrient medium and oscillated for 12 h at 37°C and 220 r/min rotational speeds, until the exponential growth phase was reached. The actual number of cells used for a given experiment was determined by the standard serial dilution method. The pure PES membrane and the hybrid membrane (membrane weight 0.03 g) were cut and sterilized by autoclaving for 20 min. To test the antibacterial activity, the membranes were added into the 5 mL solution and inoculated with about 10<sup>6</sup> CFU (colony-forming units)/mL of *E. coli*, which was then incubated at room temperature. Under the same condition, a suspension culture without any membrane was used as blank. After 24 h, membranes were retrieved from the culture and washed by normal saline. The effluent solutions were collected and diluted 1000 times with deionized water. Diluted solution (0.2 mL) was spread onto LB culture medium, and all plates were incubated at 37°C for 24 h. The numbers of colonies on the plates were determined by the plate count method and bacteriostasis rate ( $B_R$ ) was defined by the following equation:<sup>46</sup>

$$B_R = \left( \frac{n_0 - n_1}{n_0} \right) \times 100\% \quad (7)$$

where  $n_0$  is the number of colonies on the plates that treated with the pure PES membranes,  $n_1$  is the number of colonies on the plates that treated with the hybrid membranes.

## Results and discussion

### Characterization of AgNPs-HNTs-rGO

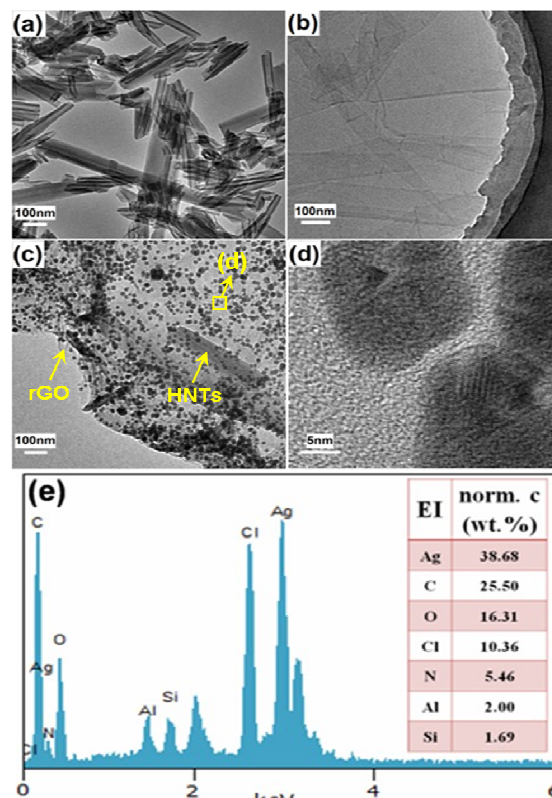


Fig. 2 TEM images of (a) HNTs, (b) GO and (c) AgNPs-HNTs-rGO nanocomposites, (d) HRTEM image of Ag nanoparticles. (e) EDS of AgNPs-HNTs-rGO nanocomposites

The microstructure of HNTs, GO nanosheets and AgNPs-HNTs-rGO nanocomposites were observed by TEM, and are shown in Fig. 2. HNTs (as shown in Fig. 2a) had a cylindrical shape and contained a transparent central area, which was longitudinal along with the cylinder, indicating that the nanotubular structures were hollow and open-ended, with a length of 0.5-2  $\mu\text{m}$ , an inner diameter of 20-30 nm and a shell thickness of 15-20 nm. The large and smooth unhindered pores could potentially act as water flow channels within the membrane matrix, improving the membrane water flux after. Fig. 2b shows TEM image of GO nanosheets, indicating GO nanosheets tend to congregate together to form multilayer agglomerates. The individual nanosheets had sizes extending from tens to several hundreds of square nanometers. The TEM image also confirmed that GO nanosheets was successfully prepared by oxidizing natural graphite.

The sandwich-like structure of AgNPs-HNTs-rGO was confirmed by the TEM image as shown in Fig. 2c. AgNPs with 10 nm were distributed evenly on the surface of rGO nanosheets. HNTs were filled between neighboring rGO sheets as spacers. The EDS of AgNPs-HNTs-rGO nanocomposites (shown in Fig. 2e) confirmed the presence of multiple components in the nanocomposites: Si and Al for HNTs, Ag for AgNPs and C for rGO.

### Characterization of membranes

#### XPS characterization of membranes

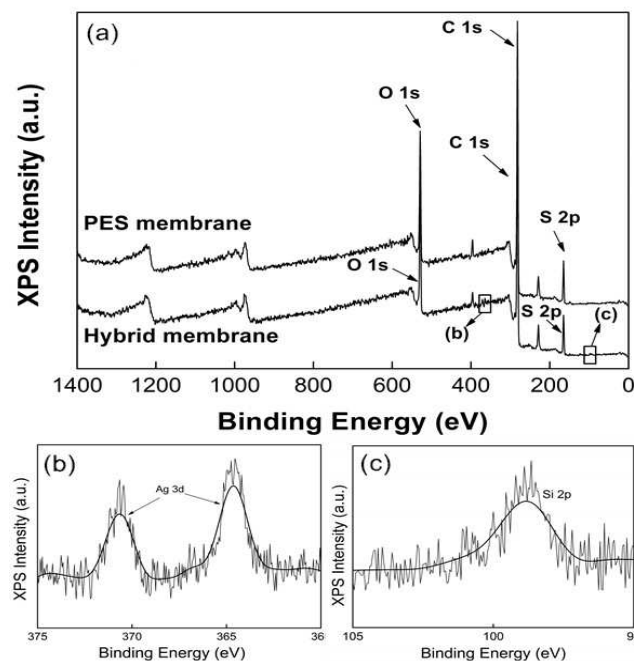


Fig. 3 XPS spectra of membrane surface: (a) PES membrane and PES/AgNPs-HNTs-rGO hybrid membrane, (b) the hybrid membrane in the region of Ag 3d, (c) the hybrid membrane in the region of Si 2p

To prove the existence of nanocomposites on the surface of the hybrid membranes, XPS characterizations of the membrane surfaces were displayed in Fig. 3. As shown in Fig. 3(a), comparing with the pure PES membrane surface, the hybrid membrane surface had extra two emission peaks at 364.55 eV (b: Ag 3d) and 98.65 eV (c: Si 2p), which confirmed the presence of Si 2p for HNTs, Ag 3d for AgNPs on the membrane surface.

#### Hydrophilicity of membranes

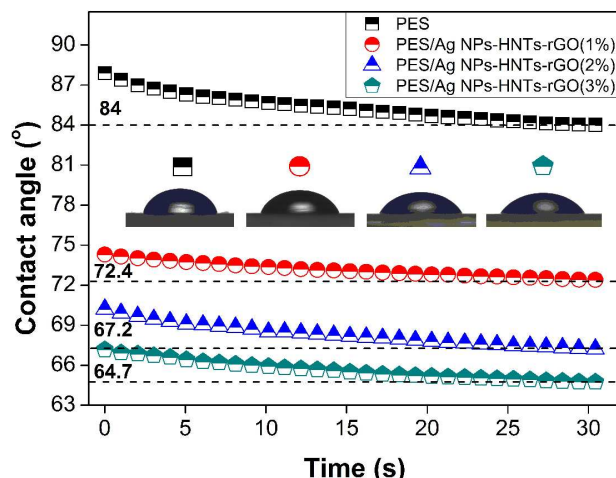


Fig. 4 Dynamic water contact angle of the membranes with various AgNPs-HNTs-rGO content

The dynamic water contact angle measurement was applied in this work to characterize the change of hydrophilic properties of the membrane surface after blending the nanocomposites. As shown in Fig. 4, the pure PES membrane had the contact angle of 84° with around 30 s due to the hydrophobic nature of the PES polymer. With the addition of the nanocomposites, the water contact angle decreased with higher nanocomposite concentration, and the variation trends of the curves of hybrid membranes were smoother compared with pure PES membrane. Such an observation indicated that the hydrophilicity of the hybrid membrane was improved due to the addition of AgNPs-HNTs-rGO nanocomposites, which could be attributed to the presence of the hydroxyl groups on HNTs. During the phase inversion process, the hydrophilic AgNPs-HNTs-rGO migrated spontaneously to the membrane/water interface to reduce the interface energy,<sup>37,55</sup> which led to higher nanocomposite exposure on the membrane surface and benefit the reduction of membrane hydrophobicity.

#### AFM images of the hybrid membrane surfaces

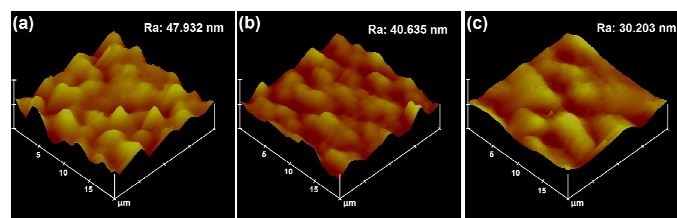


Fig. 5 AFM images of the hybrid membranes with various AgNPs-HNTs-rGO content: (a) 1 wt.%, (b) 2 wt.%, (c) 3 wt.%

The antifouling abilities of the membrane can be influenced by the roughness of membrane surface, which can be verified by the following fouling experiments. Herein, the three-dimensional AFM images of the hybrid membranes with different AgNPs-HNTs-rGO content is shown in Fig. 5. In these images, the brightest area presents the highest point of the membrane surface and the dark regions indicate valleys or membrane pores. The mean roughnesses ( $R_a$ ) of the hybrid membranes decreased from 47.9 nm for the AgNPs-HNTs-rGO concentrations of 1 wt.% to 30.2 nm for the AgNPs-HNTs-rGO concentrations of 3 wt.%, which corresponded with the

## ARTICLE

tendency of dynamic water contact angle of the membrane surfaces. The variation may be explained as the following: With the increase of AgNPs-HNTs-rGO nanomaterial in the casting solution, more hydrophilic nanomaterial migrated spontaneously to the membrane/water interface in the phase inversion process, which resulted in the more valleys of the membrane surfaces were filled with nanomaterial. It is well established that the hybrid membrane with lower roughness and surface energy has stronger antifouling abilities.

## Morphology of membranes

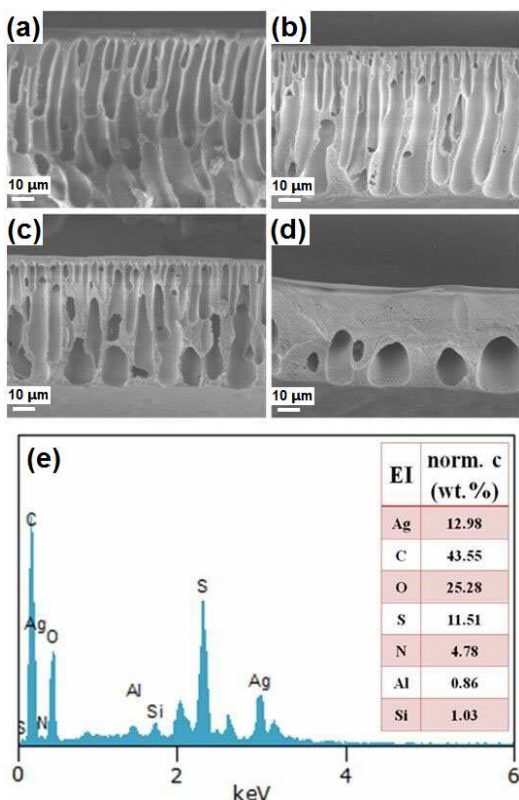


Fig. 6 SEM images of the cross-section morphology of (a) the pure PES membrane, hybrid membranes with AgNPs-HNTs-rGO concentrations of (b) 1 wt.%, (c) 2 wt.%, (d) 3 wt.%, and (e) EDS of the hybrid membrane with 2 wt.% of AgNPs-HNTs-rGO

Fig. 6 shows the morphologies of the membrane cross-section images. Compared with pure PES membrane, the addition of low concentration AgNPs-HNTs-rGO (1 wt.%) reduced the thickness of the top dense layer, but higher nanocomposite concentration led to significant increase of the top layer thickness. The addition of AgNPs-HNTs-rGO into the membrane casting solution could promote the solvent (DMAc)-non solvent (water) exchange during the membrane fabrication process due to the hydrophilic nature of the nanocomposite material, which would lead to thinner dense layer. However, higher nanocomposite concentration could increase the viscosity of the casting solution and led to slower phase separation process, resulting in a thicker layer. Furthermore, in this study, the porosity of the pure and the hybrid membranes with nanocomposite concentration of 1 wt.%, 2 wt.%, 3 wt.% were 63.9%, 60.2%, 56.7% and 51.6%, respectively. These results were consistent with membrane morphology in Fig. 6. The presence of the nanocomposite was confirmed by the EDS test of the hybrid membrane (Fig. 6e): the detection of Si, Al

and Ag elements indicated the nanocomposite was successfully incorporated into the membrane matrix. Furthermore, TEM image of the hybrid membrane (Fig. 7) revealed the tubular structure of HNTs, the lamellar structure of rGO and the spots of AgNPs inside the membrane matrix.

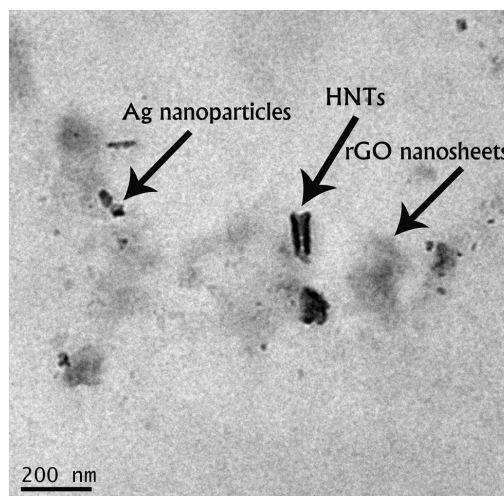


Fig. 7 TEM images of the hybrid membrane with 3 wt.% AgNPs-HNTs-rGO

## The effect of nanocomposite on the membrane performance

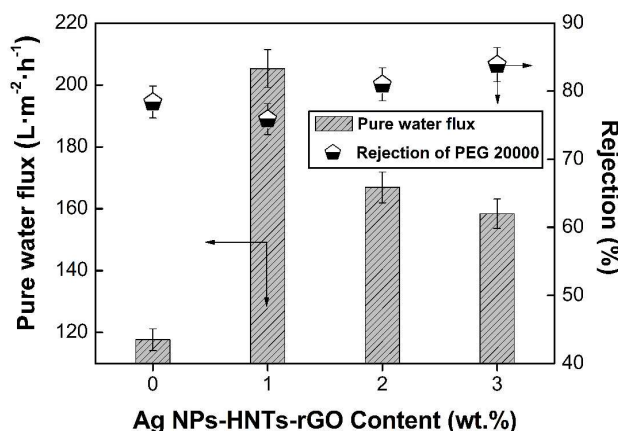


Fig. 8 Separation performances of PES membranes with different concentrations of AgNPs-HNTs-rGO nanocomposites at 25°C and 0.1 MPa

Fig. 8 shows the average pure water fluxes and the rejection rates of PEG 20000 for pure PES and hybrid membrane with different AgNPs-HNTs-rGO content. The addition of AgNPs-HNTs-rGO could significantly increase the pure water flux of the membrane. The highest flux was observed with 1 wt.% AgNPs-HNTs-rGO hybrid membrane. Further increase the nanocomposite concentration would lead to a gradual reduction of the pure water flux. For 3 wt.% AgNPs-HNTs-rGO hybrid membrane the flux was only 158.4 L/(m<sup>2</sup>·h). However, this was still about 34.6% higher than that of the pure PES membrane. On the other hand, the membrane rejection rate of PEG 20000 only had very minor change after the addition of AgNPs-HNTs-rGO, indicating the membrane pore size did not make dramatic change. This observation indicated the increase of the pure water flux could be attributed the change of membrane hydrophilicity and the formation of nanoscale flow channels

between neighboring GO sheets. The principle of the nanoscale flow channel formation was described in Fig. 9. With further increase of the AgNPs-HNTs-rGO content, the water flux decreased, which could be attributed to the increase of the dense layer thickness as shown in Fig. 6.

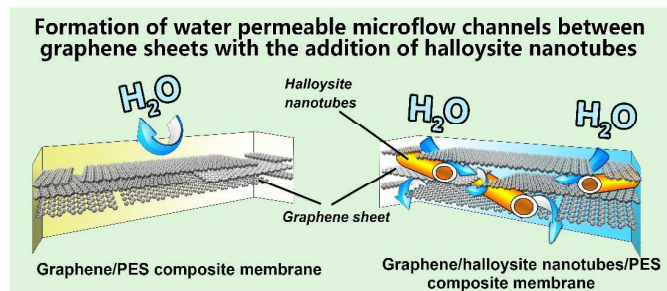


Fig. 9 Principle of increasing water flux for the PES hybrid membranes

### Antifouling performance of the membranes

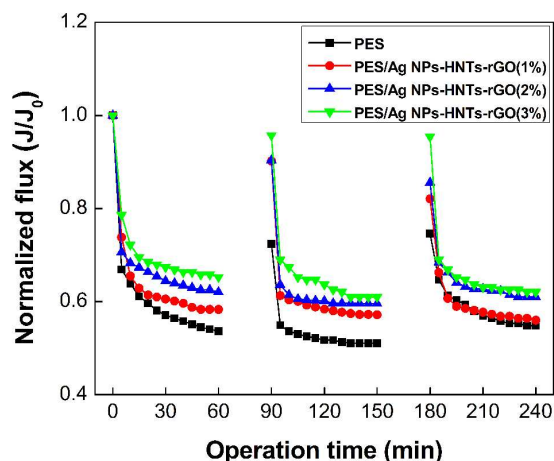


Fig. 10 Normalized flux profiles of the tested membranes during filtration of BSA solution at 25°C and 0.1 MPa

As presented above, the antifouling performance of a membrane is crucial for its long-term operational performance. In this work, both dynamic and static fouling tests were carried out. In terms of the dynamic fouling test, the normalized flux ( $J/J_0$ ) was used to evaluate the antifouling performance of the prepared membranes. Fig. 10 demonstrates that during the BSA membrane filtration process the permeation flux decreased dramatically. The most significant permeation loss was observed with pure PES membrane. Even after chemical cleaning, its initial permeation flux in each testing cycle could only return to 70% (2<sup>nd</sup> cycle) and 75% (3<sup>rd</sup> cycle) of its initial flux in the first cycle. This observation indicated the irreversible fouling occurred on the pure PES membrane, which could be attributed to the hydrophobic nature of PES polymer.<sup>56</sup> In comparison, after the addition of AgNPs-HNTs-rGO, the flux decline was less significant, and the chemical cleaning could effectively recover its initial permeation flux, indicating the improved antifouling performance of the hybrid membrane. These results could be attributed to two aspects. After the addition of AgNPs-HNTs-rGO, the membrane hydrophilicity increased (Fig. 4), which decreased the affinity between membrane surface and the proteins.

The static protein adsorption test was also conducted to explore the membrane antifouling behavior. Fig. 11 revealed the addition of

AgNPs-HNTs-rGO could effectively reduce the protein adsorption onto the membrane surface. Compared with pure PES membrane, only about half amount of BSA was adsorbed onto the 3 wt.% AgNPs-HNTs-rGO membrane. This observation was in accordance with previous dynamic fouling test, confirming the improved antifouling behavior of the hybrid membrane.

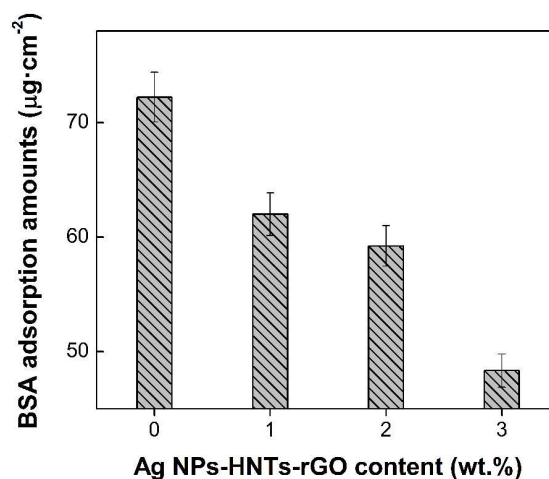


Fig. 11 BSA adsorption of the tested membranes for 24 h at 40°C (the initial concentration of BSA about 0.8 g/L)

### Antibacterial activity of the membranes

The surface morphology of the *E. coli* on the membrane was monitored by SEM and TEM to understand the antibacterial activity of the membranes. As shown in Fig. 12, the surface morphology of *E. coli* cells on pure PES membrane was intact, peritrichous and rod-shaped which indicated that the pure PES membrane had no antibacterial activity. In contrast, the morphology of a large fraction of *E. coli* cells on the hybrid membrane was significantly damaged. The TEM images also confirmed the antibacterial behavior of the hybrid membrane. After being treated with the hybrid membranes, the *E. coli* morphology changed significantly, indicating the bacteria cells on the hybrid membrane lost their integrity due to the reaction with the antibacterial agent on the membrane surface.<sup>7, 48, 56, 57</sup>

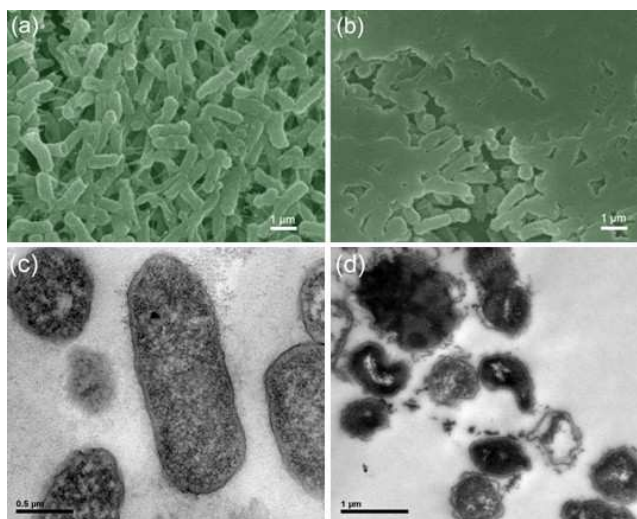


Fig. 12 SEM (a, b) and TEM (c, d) images of *E. coli* attached to membranes: (a), (c) the pure PES membrane, (b), (d) the hybrid membrane with 3 wt.% of AgNPs-HNTs-rGO (12 h incubation at 37°C)

## ARTICLE

In this work, to mimic the real working conditions, the filtration test of prepared membranes was performed using bacterial water (*E. coli*-containing feedwater) under the same conditions as the permeation test. The flux decreased greatly when *E. coli* was present in the mixed solution. As shown in Fig. 13(a), the flux dropped 67.3% from 113 to 36.9 L/(m<sup>2</sup>·h) in 24 h, denoting that the pure PES membrane could be easily fouled by *E. coli*. In contrast, the hybrid membrane displayed a lowed flux drop comparing with the pure PES membrane. The flux drop was only 19.5% from 102.7 to 82.7 L/(m<sup>2</sup>·h), which mainly due to the effect of the medium. In addition, the hybrid membrane also showed a good antibacterial property after soaking in deionized water for 20 d. It was notable that no bacterium cells were found in the permeate water samples for the pure PES and hybrid membrane, which was due to the pore size on the surface of the membranes smaller than bacterium cells, so all cells were trapped inside the filtration module, and they could further grow or be killed depending on the properties of the membrane. Herein, the concentration of living bacterium cells inside the filtration module (*i.e.*, in the reject water) was determined during filtration by the colony-counting method. As shown in Fig. 13(b), the concentration of living *E. coli* cells increased from about  $3 \times 10^6$  CFU to about  $77 \times 10^6$  CFU in the reject water when the pure PES membrane was used. In contrast, the hybrid membrane could effectively inhibit the growth of *E. coli* cells because of the AgNPs-HNTs-rGO disinfection layer, there was no significantly increase in living *E. coli* cell concentration even the hybrid membrane after soaking in deionized water for 20 d.

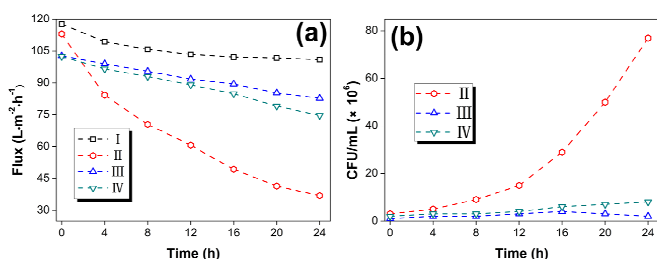


Fig. 13 The continuous filtration test: (a) the flux change with time using *E. coli*-containing feedwater and (b) viable *E. coli* cell concentration in the reject water. (I) control test of pure PES membrane using the mixed solution without *E. coli*; (II) pure PES membrane; (III) the hybrid membrane (IV) the hybrid membrane after soaking in deionized water for 20 d

The bacteriostasis rate was used to quantitatively analyze the antibacterial activity of the test membranes by the viable cell counting technique. The hybrid membrane had a high antibacterial activity against *E. coli*, and the bacteriostasis rate reached 100%. Another important issue associated with the antibacterial membrane was the gradual leaching of the immobilized active agents and the eventual loss of its activity.<sup>19</sup> As a result, the long-term antibacterial performance of the hybrid membrane was tested with bacteriostasis rate test for six months. After each test, the membrane was fully rinsed, dried and stored under room temperature. As shown in Fig. 14, the antibacterial activity still remained 90% of its original level by the end of the test, indicating the ideal long-term stability of the membrane.

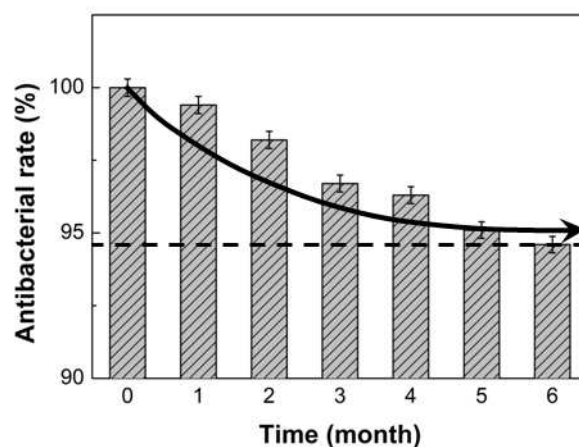


Fig. 14 Long-lasting antibacterial rate of the hybrid membranes with 3 wt.% of AgNPs-HNTs-rGO against *E. coli*

## Conclusions

A novel sandwich-like nanocomposite material was synthesized and a series of hybrid membranes were prepared by blending the nanocomposite into PES membrane matrix. The results revealed that AgNPs could be evenly immobilized onto rGO nanosheets with an average size of 10 nm, and HNTs acted as a spacer between neighbouring rGO nanosheets. After blended into the PES membrane matrix, the nanocomposite material could effectively improve the membrane surface hydrophilicity and the membrane surface smoothness. The nanocomposite formed nanoscale water flow channels inside the membrane to promote the membrane water permeation flux. This study also demonstrated the addition of the nanocomposite into membrane could effectively improve the membrane antifouling performance against protein adsorption. The results also indicated the hybrid membrane possessed ideal antibacterial capability. The treatment with the hybrid membrane could effectively damage the cell structure while the pure PES membrane showed negligible antibacterial ability. Furthermore, the bacteriostasis test revealed the hybrid membrane could completely inhibit the growth of the *E. coli* cell, and the long-terms antibacterial test confirmed the superb stability of such hybrid membranes. The hybrid membrane developed in this work has improved water flux, good antifouling and antibacterial performance. It could potentially provide a promising high efficient alternative to current polymer membrane, and its performance under real wastewater treatment conditions is needed for further investigation.

## Acknowledgements

This work was financially sponsored by the National Natural Science Foundation of China (Nos. 21376225 and 21106137), and Excellent Youth Development Foundation of Zhengzhou University (No. 1421324066). We sincerely acknowledge the financial assistance of visiting research program in University of New South Wales by the China Scholarship Council (No. 201208410135).

## Notes and references

<sup>a</sup> School of Chemical Engineering and Energy, Zhengzhou University, Zhengzhou 450001, P.R. China. E-mail: zhangyatao@zzu.edu.cn

<sup>b</sup> UNESCO Centre for Membrane Science and Technology, School of Chemical Engineering, University of New South Wales, Sydney, NSW 2052, Australia

<sup>c</sup> Ocean College, Zhejiang University of Technology, Hangzhou 310014, P.R. China

1. A.J. Brown, N.A. Brunelli, K. Eum, F. Rashidi, J.R. Johnson, W.J. Koros, C.W. Jones and S. Nair, *Science*, 2014, **345**, 72.
2. Y.H.N. Jung-Ho Yun, Roong Jien Wong and Rose Amal, *ChemCatChem*, 2013, **5**, 3060.
3. Y. Liu, X. Yue, S. Zhang, J. Ren, L. Yang, Q. Wang and G. Wang, *Sep. Purif. Technol.*, 2012, **98**, 298.
4. R. Pang, J. Li, K. Wei, X. Sun, J. Shen, W. Han and L. Wang, *J. Colloid Interface Sci.*, 2011, **364**, 373.
5. K. Zodrow, L. Brunet, S. Mahendra, D. Li, A. Zhang, Q. Li and P.J.J. Alvarez, *Water Res.*, 2009, **43**, 715.
6. Y. Liu, N. Wang and J. Caro, *J. Mater. Chem. A*, 2014, **2**, 5716.
7. J. Zhang, Y. Zhang, Y. Chen, L. Du, B. Zhang, H. Zhang, J. Liu and K. Wang, *Ind. Eng. Chem. Res.*, 2012, **51**, 3081.
8. C. Liao, P. Yu, J. Zhao, L. Wang and Y. Luo, *Desalination*, 2011, **272**, 59.
9. Y. Chen, Y. Zhang, J. Liu, H. Zhang and K. Wang, *Chem. Eng. J.*, 2012, **210**, 298.
10. R.A. Damodar, S.J. You and H.H. Chou, *J. Hazard. Mater.*, 2009, **172**, 1321.
11. X. Zhu, R. Bai, K.-H. Wee, C. Liu and S.-L. Tang, *J. Membr. Sci.*, 2010, **363**, 278.
12. C. Yao, X. Li, K.G. Neoh, Z. Shi and E.T. Kang, *J. Membr. Sci.*, 2008, **320**, 259.
13. Y.-F. Yang, H.-Q. Hu, Y. Li, L.-S. Wan and Z.-K. Xu, *J. Membr. Sci.*, 2011, **376**, 132.
14. K. Zodrow, L. Brunet, S. Mahendra, D. Li, A. Zhang, Q. Li and P.J. Alvarez, *Water Res.*, 2009, **43**, 715.
15. J.T. Trevors, *Enzyme Microb. Technol.*, 1987, **9**, 331.
16. A. Panáček, L. Kvítek, R. Prucek, M. Kolář, R. Večeřová, N. Pizúrová, V.K. Sharma, T.j. Nevěčná and R. Zbořil, *J. Phys. Chem. B*, 2006, **110**, 16248.
17. M.R. Das, R.K. Sarma, R. Saikia, V.S. Kale, M.V. Shelke and P. Sengupta, *Colloids Surf., B*, 2011, **83**, 16.
18. S. Pal, Y.K. Tak and J.M. Song, *Appl. Environ. Microbiol.*, 2007, **73**, 1712.
19. J. Hou, G. Dong, Y. Ye and V. Chen, *J. Membr. Sci.*, 2014, **452**, 229.
20. J.S. Taurozzi, H. Arul, V.Z. Bosak, A.F. Burban, T.C. Voice, M.L. Bruening and V.V. Tarabara, *J. Membr. Sci.*, 2008, **325**, 58.
21. Z. Geng, E.R. Hall and P.R. Bérubé, *J. Membr. Sci.*, 2007, **296**, 93.
22. A. Razmjou, J. Mansouri and V. Chen, *J. Membr. Sci.*, 2011, **378**, 73.
23. Z. Lin, Y. Xiao, Y. Yin, W. Hu, W. Liu and H. Yang, *ACS Appl. Mater. Interfaces*, 2014, **6**, 10775.
24. C. Ba, D.A. Ladner and J. Economy, *J. Membr. Sci.*, 2010, **347**, 250.
25. R. Yang, J. Xu, G. Ozaydin-Ince, S.Y. Wong, and K.K. Gleason, *Chem. Mater.*, 2011, **23**, 1263.
26. J. Hou, G. Dong, Y. Ye and V. Chen, *J. Membr. Sci.*, 2014, **469**, 19.
27. Y. Chang, C.-Y. Ko, Y.-J. Shih, D. Quémener, A. Deratani, T.-C. Wei, D.-M. Wang and J.-Y. Lai, *J. Membr. Sci.*, 2009, **345**, 160.
28. B. Deng, M. Yu, X. Yang, B. Zhang, L. Li, L. Xie, J. Li and X. Lu, *J. Membr. Sci.*, 2010, **350**, 252.
29. M.N. Abu Seman, M. Khayet and N. Hilal, *Desalination*, 2011, **273**, 36.
30. T.N. Lambert, *J. Phys. Chem. C*, 2009, **113**, 19812.
31. F. Zhang, W. Zhang, Y. Yu, B. Deng, J. Li and J. Jin, *J. Membr. Sci.*, 2013, **432**, 25.
32. V. Vatanpour, S.S. Madaeni, R. Moradian, S. Zinadini and B. Astinchap, *Sep. Purif. Technol.*, 2012, **90**, 69.
33. H. Wu, J. Mansouri and V. Chen, *J. Membr. Sci.*, 2013, **433**, 135.
34. H. Yu, X. Zhang, Y. Zhang, J. Liu and H. Zhang, *Desalination*, 2013, **326**, 69.
35. J. Huang, H. Wang and K. Zhang, *Desalination*, 2014, **336**, 8.
36. A. Qin, X. Wu, B. Ma, X. Zhao and C. He, *J. Membr. Sci.*, 2014, **49**, 7797.
37. V. Vatanpour, S.S. Madaeni, L. Rajabi, S. Zinadini and A.A. Derakhshan, *J. Membr. Sci.*, 2012, **401-402**, 132.
38. L. Yan, Y.S. Li and C.B. Xiang, *Polymer*, 2005, **46**, 7701.
39. S. Majeed, D. Fierro, K. Buhr, J. Wind, B. Du, A. Boschetti-de-Fierro and V. Abetz, *J. Membr. Sci.*, 2012, **403-404**, 101.
40. P. Daraei, S.S. Madaeni, N. Ghaemi, M.A. Khadivi, B. Astinchap and R. Moradian, *J. Membr. Sci.*, 2013, **444**, 184.
41. J. Zhu, N. Guo, Y. Zhang, L. Yu and J. Liu, *J. Membr. Sci.*, 2014, **465**, 91.
42. S. Azari and L. Zou, *J. Membr. Sci.*, 2012, **401-402**, 68.
43. S. Liu, T.H. Zeng, M. Hofmann, E. Burcombe, J. Wei, R. Jiang, J. Kong and Y. Chen, *ACS Nano*, 2011, **5**, 6971.
44. J. Chen, H. Peng, X. Wang, F. Shao, Z. Yuan and H. Han, *Nanoscale*, 2014, **6**, 1879.
45. B.P. Frank and G. Belfort, *Langmuir*, 2001, **17**, 1905.
46. L. Yu, Y. Zhang, B. Zhang, J. Liu, H. Zhang and C. Song, *J. Membr. Sci.*, 2013, **447**, 452.
47. W.-P. Xu, L.-C. Zhang, J.-P. Li, Y. Lu, H.-H. Li, Y.-N. Ma, W.-D. Wang and S.-H. Yu, *J. Mater. Chem.*, 2011, **21**, 4593.
48. J. Ma, J. Zhang, Z. Xiong, Y. Yong and X.S. Zhao, *J. Mater. Chem.*, 2011, **21**, 3350.
49. H. Yu, Y. Zhang, X. Sun, J. Liu and H. Zhang, *Chem. Eng. J.*, 2014, **237**, 322.
50. Y. Chen, Y. Zhang, H. Zhang, J. Liu and C. Song, *Chem. Eng. J.*, 2013, **228**, 12.
51. Z. Wang, H. Wang, J. Liu and Y. Zhang, *Desalination*, 2014, **344**, 313.
52. Y. Zhang, Y. Chen, H. Zhang, B. Zhang and J. Liu, *J. Inorg. Biochem.*, 2013, **118**, 59.
53. D.C. Marciano, D.V. Kosynkin, J.M. Berlin, A. Sinitskii, Z. Sun, A. Slesarev, L.B. Alemany, W. Lu and J.M. Tour, *ACS Nano*, 2010, **4**, 4806.
54. J. Hong, D. Xu, P. Gong, H. Sun, L. Dong and S. Yao, *J. Mol. Catal. B: Enzym.*, 2007, **45**, 84.
55. E. Celik, H. Park and H. Choi, *Water Res.*, 2011, **45**, 274.
56. I. Sawada, R. Fachrul, T. Ito, Y. Ohmukai, T. Maruyama and H. Matsuyama, *J. Membr. Sci.*, 2012, **387-388**, 1.
57. X. Cao, M. Tang, F. Liu, Y. Nie and C. Zhao, *Colloids Surf. B: Biointerfaces*, 2010, **81**, 555.